

Droplet size spectra and water-vapor concentration of laboratory water clouds: inversion of Fourier transform infrared (500–5000 cm^{-1}) optical-depth measurement

W. Patrick Arnott, Carl Schmitt, Yangang Liu, and John Hallett

Infrared extinction optical depth (500–5000 cm^{-1}) has been measured with a Fourier transform infrared spectrometer for clouds produced with an ultrasonic nebulizer. Direct measurement of the cloud droplet size spectra agree with size spectra retrieved from inversion of the extinction measurements. Both indicate that the range of droplet sizes is 1–14 μm . The retrieval was accomplished with an iterative algorithm that simultaneously obtains water-vapor concentration. The basis set of droplet extinction functions are computed once by using numerical integration of the Lorenz–Mie theory over narrow size bins, and a measured water-vapor extinction curve was used. Extinction and size spectra are measured and computed for both steady-state and dissipating clouds. It is demonstrated that anomalous diffraction theory produces relatively poor droplet size and synthetic extinction spectra and that extinction measurements are helpful in assessing the validity of various theories. Calculations of cloud liquid-water content from retrieved size distributions agree with a parameterization based on optical-depth measurements at a wave number of 906 cm^{-1} for clouds that satisfy the size spectral range assumptions of the parameterization. Significance of droplet and vapor contribution to the total optical depth is used to evaluate the reliability of spectral inversions. © 1997 Optical Society of America

1. Introduction

Early measurements¹ of the infrared optical depth of natural fog and haze were performed at a few wavelengths (1.24, 1.7, 3.7, and 10 μm) and were away from strong water-vapor absorption bands. These measurements revealed definite spectral variability, especially a reduction in optical depth at 10 μm compared with the optical depth at 2 μm . Qualitative agreement was achieved among measured optical-depth spectra and optical-depth spectra modeled with Lorenz–Mie-theory. Haze and fog were defined in terms of the measured optical depth, though haze (e.g., light fog in modern parlance) generally also turned out to have most water droplets in the diameter range below 16 μm . This diameter range also covers the range of droplet sizes observed in our measurements. One conclusion from the early work was

that IR emission from warm bodies could be sensed more readily in haze (e.g., light fog) than in fog owing to the differences in optical depth at 10 μm . Infrared extinction measurements and calculations for hazes, fogs, and water clouds have been performed by a large number of researchers since the early measurements.^{2–13}

These early and subsequent measurements were used to retrieve droplet size spectra from spectral optical-depth measurements.^{14,15} While it is now well known^{16,17} that the integral equation used in the retrieval is ill posed in the sense that a wide range of aerosol size spectra produce basically the same synthetic extinction spectra, not just any assumed size spectra produce synthetic extinction spectra in good agreement with measured spectra.¹⁴ Indeed, Eldridge was able to retrieve droplet size spectra and produced synthetic optical-depth spectra in reasonable agreement with measured values, even though incorrect water refractive-index values were used.¹⁴ Penndorf was quick to point out that the retrieval was not unique.¹⁸ Eldridge argued that the retrieval was still useful and that better measurements would probably help.¹⁹ This same sense of utility has motivated much development in retrieving a

The authors are with the Atmospheric Sciences Center, Desert Research Institute, P. O. Box 60220, Reno, Nevada 89506.

Received 17 June 1996; revised manuscript received 24 October 1996.

0003-6935/97/215205-12\$10.00/0

© 1997 Optical Society of America

wide variety of information from spectral measurements.¹⁶ Schemes for retrieving aerosol-droplet size spectra from optical-depth measurements are still of contemporary interest.²⁰ Although a subset of our basic goals are similar to the early studies, we have the advantages of improved spectrometer technology to cover a much wider spectral range at higher resolution, of improved knowledge of the refractive index of water, and of the algorithms necessary for reliable retrievals. An additional goal not considered in the early studies is to retrieve droplet size spectra simultaneously with water-vapor concentration.

Spectral extinction measurements have been used to retrieve refractive indices of particulate ice when the shape of particle size spectra can be assumed.²¹ Emission along with transmission measurements have been used to estimate size spectra of combustion particles as well as the concentration of various gases, although the size spectrum was assumed to be given by an analytical expression with a few adjustable parameters.²² While *a priori* knowledge of particle size spectra can simplify subsequent analysis, such knowledge is not always available. By contrast, a retrieval scheme will be described here that gives both droplet size spectra and water-vapor concentration with no *a priori* knowledge of the size spectra assumed, other than a gross estimate of range of particle sizes.

A commonly discussed method for inverting spectral extinction measurements uses analytical inversion^{23–28} to determine the size distribution. This method uses the van de Hulst anomalous diffraction theory approximation²⁹ for spherical particles. Comparisons of the approximate inversions with the exact Lorenz–Mie theory are sparse, although one such comparison²⁸ apparently motivated an empirical improvement of the anomalous diffraction theory model that actually did produce retrieved size spectra in reasonable agreement with Lorenz–Mie theory results. We found that the anomalous diffraction approximation produced unsatisfactory results when applied in our numerical retrieval scheme in comparison with those retrieved from the Lorenz–Mie theory.

The approach we took was to measure IR extinction and droplet size spectra for artificial water clouds as described in Section 2 and to retrieve droplet size spectra, using an iterative algorithm described in Section 3. Our goals in these measurements are to demonstrate the feasibility of retrieving droplet spectra and water-vapor concentration from IR extinction measurements made with a Fourier transform infrared (FTIR) spectrometer, with possible application to natural haze (sufficiently water diluted), fog, and water cloud droplet retrieval, and to demonstrate that measurements can help determine the validity of models for extinction. Natural haze and fog can obscure long-path FTIR measurements of trace gases. The results may assist in accurate assessment of obscuration by haze and fog and perhaps extend the information content retrievable by these measurements.

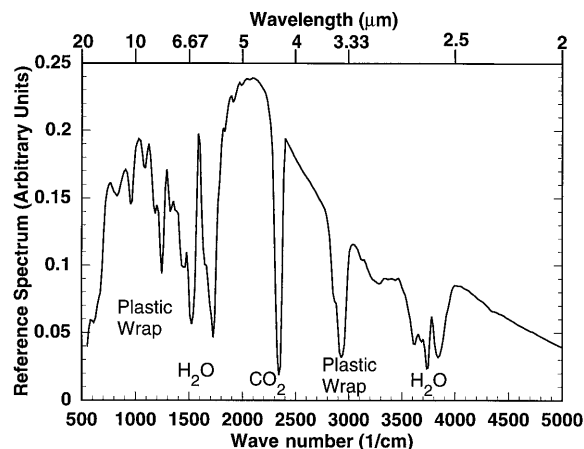


Fig. 1. Typical reference spectrum taken with no cloud present.

2. Measured and Retrieved Droplet Size and Extinction Optical-depth Spectra

A. Measurement Procedures

Much of the experimental arrangement used for IR extinction measurements has been described³⁰ in a previous publication, although some changes were made to accommodate measurements of water clouds. Briefly, the FTIR was used as a transmission spectrometer. A broad band IR source already modulated by the Michelson interferometer in the FTIR spectrometer was reflected by a concave mirror in the 1-m³ cloud chamber into a nearly collimated detector located at twice the focal distance of the mirror. A reference spectrum was taken with no cloud present, and the optical depth for a cloud was determined by taking the logarithm of the transmission measurement (ratio of cloud and no-cloud spectra). It was determined that the 32-cm⁻¹ resolution setting on the FTIR spectrometer gave sufficient resolution and signal-to-noise discrimination for the vapor and droplet spectral measurements. Cloud droplets were produced with an ultrasonic nebulizer, more commonly known as ultrasonic humidifiers for routine household use (Sunbeam Model 694), and droplets were delivered to the chamber via a 2.54-cm-diameter polyethylene corrugated hose used to direct the droplet-laden air stream issuing from the device.

An example reference spectrum is shown in Fig. 1. Radiation is absorbed in some bands by water vapor and carbon dioxide present in the air between the IR source and the detector and by the plastic wrap used both as a window and to confine the cloud in the chamber. The plastic wrap was stretched thin to reduce IR absorption and to make it tight over the opening in the chamber. It was heated by a warm air stream from outside the chamber to prevent condensation, while the concave mirror inside the chamber was heated from its back side with an attached film heater for the same purpose. Temperature changes in the chamber or surrounding air occurring between acquisition of the reference and the transmission spectrum also change the concentration of

absorbing molecules and hence potentially alter the optical-depth results in selected bands. Even slight changes of droplet temperature in the cloud result in appreciable water-vapor concentration changes. The effects of such temperature changes are evident in the optical depth spectra discussed below.

Although the ice clouds studied previously³⁰ had water-vapor concentration essentially at ice saturation at the chamber temperature during both the reference- and the cloud spectrum measurements, the vapor concentration for water clouds was variable. The vapor concentration was driven near water saturation at the chamber temperature for the reference measurement by shallow pans of water placed in the bottom of the chamber. This procedure was followed by several cycles of cloud injection and dissipation. To test vapor concentration, a reference spectrum was taken before a new cloud was injected and an optical-depth measurement was taken after the cloud had dissipated. Eventually the chamber approached water saturation as judged by the lack of optical-depth change.

The degree of control of cloud characteristics was not a major concern. Clouds were obtained that reached a steady state, or evaporated in a nonsteady state, to give drop spectra and changes of drop spectra suitable for evaluating the retrieval. Under steady-state conditions an equilibrium was established between droplet input to the chamber and droplet evaporation along with gravitational settling. Air near the chamber walls was at or below water saturation (depending on the presence or absence of water on the walls) with respect to a flat surface of water. Even if air near the walls was locally at water saturation, droplets still would evaporate to the walls because of the Kelvin effect³¹ (enhanced vapor pressure of the droplets with increasing radius of curvature). This is significant for droplets of diameter up to approximately 10 μm for times of order 500 s at a distance up to approximately 5 cm of the walls. For droplets above this size, fallout becomes significant on these time scales. Some of the factors that influenced chamber air temperature were the room temperature, the relative humidity of air entering the nebulizer, and the heater that was used to prevent condensation on the mirror. Under nonsteady-state conditions following shutoff of the nebulizer, turbulence levels decreased to approximately 1 cm/s, and droplet numbers decreased as evaporation took place to the walls over a period of several hundred seconds. After this period a haze remained and probably was controlled by impurity reduction of vapor pressure.

To yield a water-vapor optical-depth spectrum for use in the retrieval algorithm, a reference spectrum was taken with significantly undersaturated air. Temperature and relative humidity were measured with a Vaisalla probe and were used to compute water-vapor density. Then the water-vapor density was increased by the addition of droplets to the chamber, the droplets quickly evaporated in the dry air. Temperature and relative humidity were again mea-

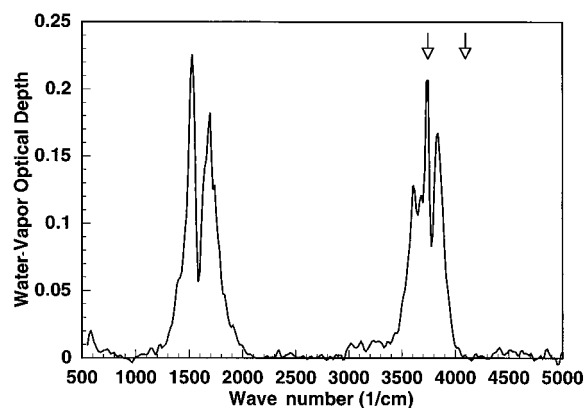


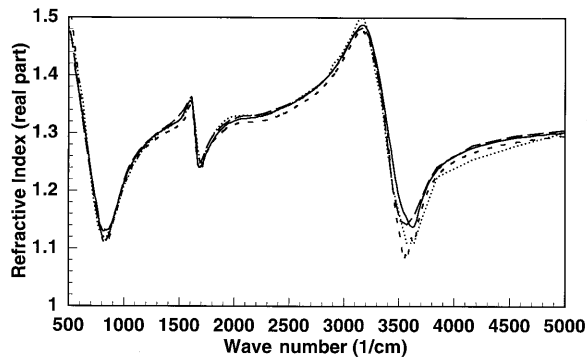
Fig. 2. Measured water-vapor spectrum at 32-cm^{-1} resolution for a vapor-density increase of 5.2 g/m^3 . Arrows indicate wave numbers of the comparison in Fig. 6.

sured, and the vapor-density increase was determined. The water-vapor spectrum was then obtained by taking the transmission measurement. Figure 2 shows the measured water-vapor spectrum for a vapor-density increase of 5.2 g/m^3 . The individual lines that can be resolved at higher spectral resolution are averaged out at the coarse resolution of 32 cm^{-1} used for the measurement, although this resolution is quite adequate for the condensed phase of water because the absorption spectra are quite broad. Both the reference and the transmission spectra were averages of 10 spectra each, and the undulation in the low-optical-depth part of the spectrum between 2500 and 2900 cm^{-1} in Fig. 2 indicates the typical noise level in the measurement.

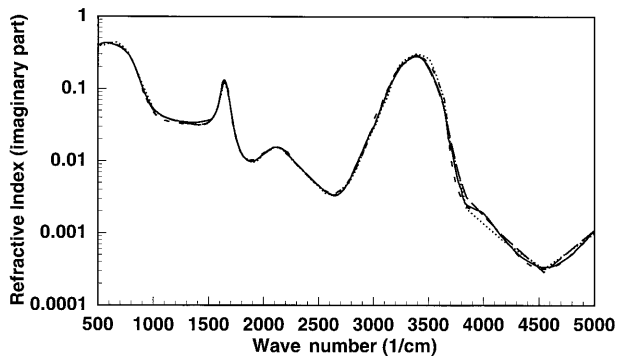
The refractive index of bulk water as determined by three groups^{32–35} is shown in Fig. 3. The real part of the refractive index in Fig. 3(a) shows several minima that correspond to reduced extinction³⁰ by water droplets that is due to a reduction in scattering because of a real refractive index that is close to that of air. The imaginary part of the refractive index shown in Fig. 3(b) determines absorption by bulk water and is slower varying than optical depth for water vapor shown in Fig. 2. The refractive-index tabulation given in Ref. 32 produced synthetic extinction spectra for water droplets in better agreement with the measured spectra than did the others. The variability shown in Fig. 3 perhaps leads one to question the current knowledge of the refractive index for water.

B. Steady-state Cloud

The nebulizer was operated continuously at a low setting so that after 5–10 minutes a steady-state droplet cloud was achieved. Optical depth was monitored in the visible with a 685-nm laser diode and indicated fluctuations from the average optical depth of $\sim 5\%$ for the steady-state clouds. Steady-state equilibrium was achieved when the rate of droplet addition matched the rate of droplet removal. The nebulizer fan resulted in air motion within the cham-



(a)



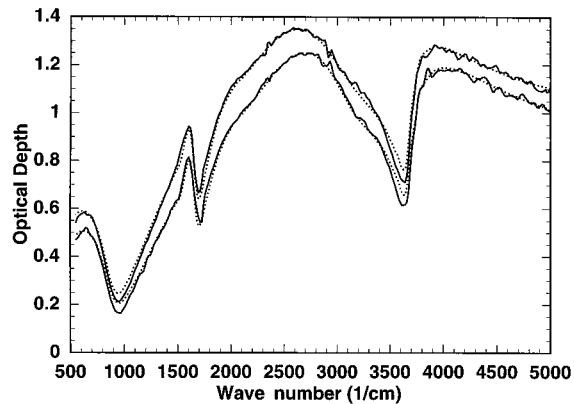
(b)

Fig. 3. Refractive index of water as a function of wave number. Solid, long-dashed, dotted, and short-dashed curves are from Refs. 32, 33, 34, and 35, respectively.

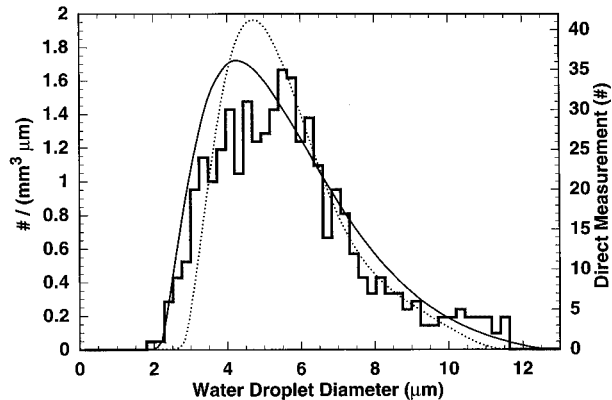
ber of approximately 2 cm/s, which carried droplets to the chamber walls and floor.

Figure 4(a) shows measured and synthetic optical-depth spectra of water droplets for two settings of the ultrasonic nebulizer. All synthetic spectra discussed in this section were computed by the retrieval algorithm with smoothing as described in Section 3. The agreement between measured and modeled spectra is worse near the spectral regions of disagreement for the real part of the refractive index from the various references, plotted in Fig. 3(a). The lack of smoothness in the measured spectra between 4000 cm^{-1} and 5000 cm^{-1} is due to the relatively high optical depth and relatively low source-spectral energy (Fig. 1). Low spectral energy that is due to carbon dioxide and plastic-wrap absorption contributed to the lack of smoothness between 2300 and 2400 cm^{-1} and between 2900 and 3000 cm^{-1} , respectively. The reference spectra were averages of 10 and 5000 FTIR scans and the transmission spectra were averages of 100 and 5000 FTIR scans for the lower and the higher optical-depth measurements, respectively. The extra averaging for the higher optical-depth case perhaps resulted in smoother spectra between 500 and 1500 cm^{-1} . Ten FTIR scans were accomplished in approximately 4 s.

Figure 4(b) shows the retrieved droplet-size distributions that gave the synthetic optical-depth spectra in Fig. 4(a). The higher nebulizer setting appar-



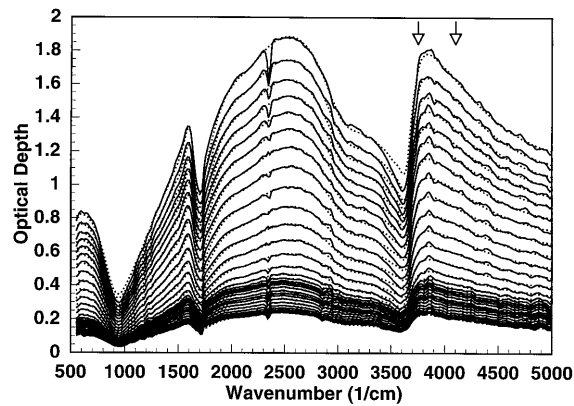
(a)



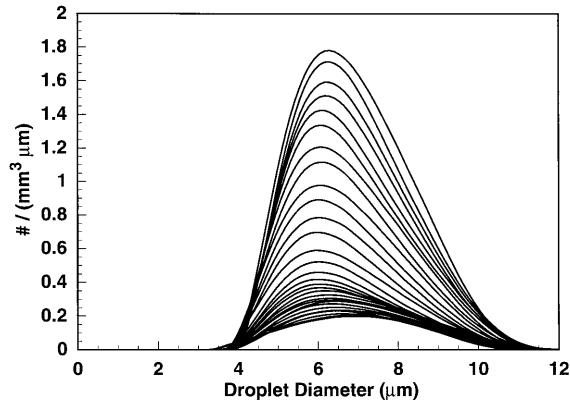
(b)

Fig. 4. (a) Optical depth for two settings of the ultrasonic nebulizer as a function of wave number measured (solid curves) and modeled (dotted curves) by means of Lorenz-Mie theory. (b) Water droplet measured counts (solid binned curve) and concentration retrieved by inversion of the greater and lesser optical depths of a) (thin solid and dotted curves, respectively).

ently corresponds to a broader droplet-size spectrum than the lower setting. Also shown in Fig. 4(b) is a direct measurement of the droplet-size distribution performed with a magnesium-coated slide³⁶ passed through the droplets very near the nebulizer, and a microscope equipped with a calibrated grid to count and size droplet images. The collection efficiency was enhanced by our rapidly moving the hand-held slide through the droplets at a few meters per second and turning the slide edge on so that one of the edges along the length of the slide was first to pass through the droplets. The computed Stokes number suggests that droplets with diameters greater than a micrometer were captured. Droplet diameters were determined directly from the measured circle diameters seen under the microscope, even though Ref. 36 recommends scaling from circle diameters to spheres by multiplying measured diameters by 0.86 for droplets larger than 5 μm and by an unknown factor greater than unity for circles less than 5 μm . Reference 36 cautions against this technique for droplets smaller than 5 μm diameter because of the typical grain size achieved when magnesium is burned to



(a)



(b)

Fig. 5. (a) Optical depth [curves as in Fig. 4(a)] and (b) retrieved droplet spectra for a dissipating fog. The time elapsed between adjacent spectra was 6 s. Arrows in (a) indicate wave numbers of the comparison in Fig. 6.

coat the slide, although by trial and error we found that grain size could be reduced enough that smaller circles were reasonably discernible. It should be emphasized that the nebulizer setting for the direct measurement was similar to the settings used to obtain the spectra in Fig. 4(a), although the direct measurement was performed on droplets collected directly from the outflow of the 2.54-cm tube connected to the nebulizer. The direct measurement was labor intensive and was performed on only one occasion. Direct measurement was also attempted by use of a forward-scattering spectrometer probe (FSSP) (manufactured by Particle Measuring Systems) equipped with an aspiration fan, although the results were sensitive to the distance between the inlet of the FSSP and the nebulizer outlet. It seemed that the forced outflow of droplets from the nebulizer and forced inflow at the FSSP resulted in highly variable droplet concentrations. It was not desirable to place the FSSP in the cloud chamber because of the aspiration fan.

C. Dissipating Cloud

Figure 5(a) shows 30 measured and synthetic spectra for a dissipating cloud that was produced by first

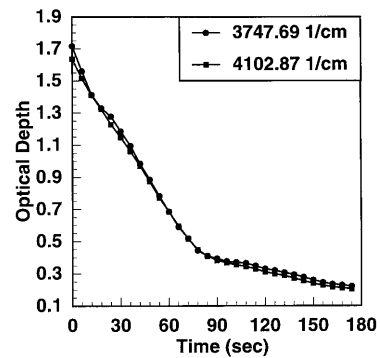


Fig. 6. Measured optical depth as a function of time at a strong absorption wave number of water vapor (3747.69 cm^{-1}) and at a nearby less absorbing wave number (4102.87 cm^{-1}). The strongest influence of water-vapor-density changes is seen as a dip before 30 s in the 3747.69-cm^{-1} curve. Curves are guides to the eye.

operating the nebulizer at maximum output and then turning it off. The first measurement was acquired 3 min after the nebulizer was turned off, to allow sufficient time for the visible optical depth to decrease to near unity. Adjacent spectra were taken every 6 s. Ten FTIR scans were averaged for each measurement. The spectra at the highest optical depth are significantly different from the spectra in Fig. 4(b). In particular, the slopes between 3000 and 3500 cm^{-1} and those between 4000 and 4500 cm^{-1} are quite different. Multiple scattering is not likely to be significant even though the optical depths in Fig. 5(a) can be in excess of 1.8, because the appreciable imaginary component of the refractive index suppresses it.³⁰ The retrieved droplet-size distribution is shown in Fig. 5(b), where the curve with the greatest number concentration corresponds to the greatest optical depth in Fig. 5(a).

The qualitative influence of water vapor on optical-depth spectra can be assessed by comparing spectra at wave numbers corresponding to strong and weak absorption by water vapor (see the arrows in Figs. 2 and 5(a) that indicate the wave numbers). Figure 6 shows the optical depth at two such wave numbers for the dissipating-cloud case in Fig. 5(a). Water-vapor absorption is strong at 3747.69 cm^{-1} , as shown in Fig. 2, and is weak at 4102.87 cm^{-1} . The reduction in optical depth at 3747.69 cm^{-1} occurring at $\sim 15 \text{ s}$ corresponds to a local, temporary reduction in water-vapor density that is likely due to turbulent mixing. The quantitative retrieval of water-vapor density shown in Fig. 7, obtained from use of the algorithm discussed in Section 3, also shows a reduction in water-vapor concentration at $\sim 15 \text{ s}$.

Some speculations about the nature of the dissipating cloud are worth elaboration. The chamber temperature after humidification was typically $22 \text{ }^\circ\text{C}$ as measured with a linear vertical array of eight thermocouples that were shielded from direct contact with droplets. The procedure described above nearly saturates the air in the chamber because, after droplets are introduced for the transmission mea-

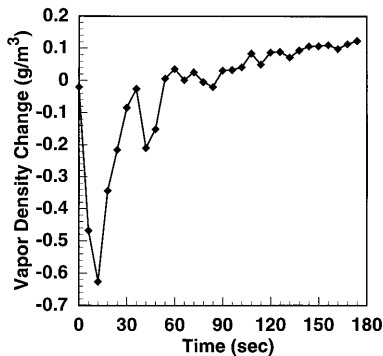


Fig. 7. Water-vapor-density-change as a function of time retrieved from the measured optical depth in Fig. 5(a). The curve is a guide to the eye.

surement, the temperature change is at most 0.2 °C. Droplets entering the chamber will be close to the wet-bulb temperature, which is ≤ 22 °C, although variations of room temperature and heat produced by nebulization affected this temperature. The saturation-vapor-pressure reduction for a droplet changing temperature by -1 °C is approximately -6% relative to the value at 23 °C. This and the introduction of relatively cool, dry, laboratory air into the nebulizer are likely to be the cause of the reduction in water vapor for a newly dissipating cloud. When the nebulizer is operating, air motion of ≈ 60 – 300 cm/min transports droplets to the vicinity of the walls, where they are evaporated, and to the floor of the chamber, although the cloud is visibly more stable when the nebulizer is not operating and the cloud is dissipating. Stokes law³¹ gives a droplet fall velocity $v_s = 0.19D^2$ cm/min, where D is the droplet diameter expressed in micrometers, so that 1- and 10- μm -diameter droplets fall at a rate of $v_s = 0.19$ cm/min and $v_s = 19$ cm/min, respectively. The Kelvin curvature effect³¹ causes a modest 0.084% and 0.095% supersaturation for the equilibrium vapor pressure of a 1- μm droplet relative to that of 5- μm and 10- μm -diameter droplets, respectively, and thus perhaps causes a slight tendency for the smaller water droplets to evaporate more rapidly than the larger droplets, as discussed in Subsection 2.A. The droplet-size distributions in Fig. 5(b) indicate that the optical-depth decrease with time in Fig. 5(a) is primarily due to droplets leaving the chamber by evaporation to the walls and deposition on the floor owing to gravitational settling and air motion. Evaporation far from walls is less important because the chamber is nearly saturated before droplets are added, although as the cloud dissipates a slight tendency toward increased vapor concentration is indicated in Fig. 7.

Liquid-water content as computed from the size distributions for the dissipating cloud is shown in Fig. 8. Also shown is the liquid-water content derived from optical-depth measurements and theory near 11- μm wavelength (≈ 906 cm^{-1}) derived from the use of Chylek's parameterization,^{37,38} which links liquid-water content directly to optical-depth measure-

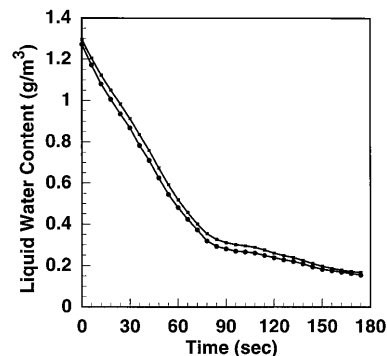


Fig. 8. Cloud liquid-water content as a function of time computed from droplet size spectra (filled circles) shown in Fig. 5(b) and from Chylek's parameterization given in Eq. (1) as computed from the measured IR spectra (filled squares). Curves are guides to the eye.

ments through the relation $\sigma_e = 128w$, where σ_e (inverse kilometers) is the extinction optical depth and w (grams per cubic meter) is the liquid-water content. The parameterization used here takes into account the $L = 2$ -m path length of radiation in the chamber and is given by

$$w = 3.91\tau(\nu = 906 \text{ cm}^{-1}), \quad (1)$$

where w is liquid water content in grams per cubic meter and $\tau(\nu = 906 \text{ cm}^{-1})$ is the measured or modeled optical depth at a $\nu = 906 \text{ cm}^{-1}$ wave number. If one considers that the constant of proportionality in Eq. (1) is an approximation^{37,38} the agreement between parameterized liquid-water content from a single wave-number measurement and retrieved liquid-water content from inversion of the entire spectrum is quite good (within 2–12%). The rate of change of liquid water significantly diminishes between 60 and 90 s, which is likely due to the reduction of turbulent mixing and vapor transport to the walls.

The total concentration and mean diameter for the dissipating cloud as computed from the size distributions in Fig. 5(b) are shown in Fig. 9. The mean diameter curve suggests that the cloud in the IR

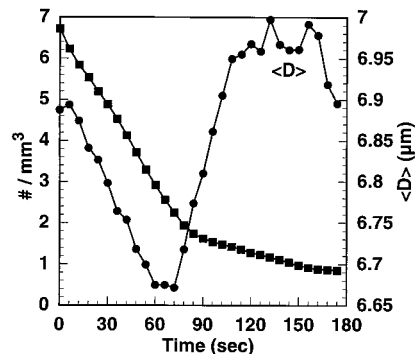


Fig. 9. Total number concentration (filled squares, left axis) and mean diameter (filled circles, right axis) as a function of time for the dissipating fog as computed from the size spectra of Fig. 5(b). Curves are guides to the eye.

beam between 60 and 120 s has been depleted of smaller droplets, which is likely due to the Kelvin curvature effect discussed earlier that hastens evaporation of smaller droplets near walls.

3. Iterative Algorithm for Gas Concentration and Droplet-size Spectra Retrieval

A. Algorithm Description

The general iterative algorithm for gas concentration and droplet size spectra retrieval will be given in this section along with some discussion of the nonuniqueness of retrieved size distributions and how this minimally affects the retrieved water-vapor concentration. Use of anomalous diffraction theory as an approximation for Lorenz–Mie theory will be shown to retrieve droplet size spectra and vapor concentration in substantial disagreement with results retrieved from the more accurate Lorenz–Mie theory.

Optical depth is due to concentration changes of water droplets and absorbing gases introduced by addition of such species or as a result of temperature changes that affect gas concentration and the saturation vapor pressure of water. Spectral optical depth $\tau(\nu)$ is modeled by

$$\tau(\nu) = L \left[\sum_{i=1}^N n(D_i) \sigma(D_i, \nu) + \sum_{i=1}^{N_g} n_{gi} \sigma_{gi}(\nu) \right], \quad (2)$$

where ν is the wave number, L is the total path length in the cloud, N is the total number of droplet-size bins with individual bins having concentrations $n(D_i)$ given in dimensions of inverse volume, $\sigma(D_i, \nu)$ is the bin-averaged droplet-extinction cross section given in dimensions of area, N_g is the total number of gases, and the product $n_{gi} \sigma_{gi}(\nu)$ is the measured or modeled extinction coefficient for the i th gas given in dimen-

sions of inverse length. The bin-averaged droplet-extinction cross section is computed from numerical integration of the equation

should be computed by use of the well-known Lorenz–Mie theory for spherical particles, although it was also computed by the simpler, less exact anomalous diffraction theory²⁹ to illustrate the sensitivity of the droplet size-spectra retrieval to the accuracy of extinction theory.

The inverse problem is theoretically solved when droplet and gas concentrations are determined by solution of Eq. (2) for n_{gi} and $n(D_i)$. Unfortunately, small measurement errors, inaccurate refractive-index values, and computational precision all conspire to render Eq. (2) ill posed in the sense that a variety of droplet concentrations will produce essentially the same quality synthetic optical-depth spectra. However, this variety of droplet size spectra retrievable with essentially the same precision is not arbitrary. The spectra typically have very similar moments of the distributions. Direct measurement of droplet spectra by impaction or some optical means such as scattering is typically performed on a drop-by-drop basis and is a statistical problem as well. Direct measurement of only one droplet to form a distribution is absurd, as is waiting forever to count an infinite number of droplets to provide perfect statistical inference of the spectrum of droplets.

The guiding principles used here to invert Eq. (2) are that the algorithm should produce synthetic optical-depth spectra in good agreement with measured quantities and that droplet size-distribution smoothing by the algorithm is acceptable as long as it does not destroy the good agreement. After some exploration of algorithms, the one chosen was an iterative algorithm that determines a new estimate for the concentration of the k th droplet size bin or gas concentration $n_k^{(new)}$ through use of the equation

$$n_k^{(new)} = \frac{\sum_{j=1}^{N_v} \sigma(S_k, \nu_j) \left[\frac{\tau_m(\nu_j)}{L} - \sum_{i=1}^{k-1} n_i^{(old)} \sigma(S_i, \nu_j) - \sum_{i=k+1}^{N_t} n_i^{(new)} \sigma(S_i, \nu_j) \right]}{\sum_{j=1}^{N_v} \sigma(S_k, \nu_j)^2}, \quad (4)$$

sions of inverse length. The bin-averaged droplet-extinction cross section is computed from numerical integration of the equation

$$\sigma(D, \nu) = \frac{1}{\Delta D} \int_{D_i - \Delta D/2}^{D_i + \Delta D/2} \sigma(D, \nu) dD \quad (3)$$

where $\sigma(D, \nu)$ is the extinction cross section for a droplet of diameter D and for wave number ν . The solution of Eq. (2), of course, requires knowledge of the droplet complex refractive index, which for water was taken from Ref. 32. Notice that it is somewhat artificial to single out gas and droplet contributions to extinction in Eq. (2). The extinction cross section

where the index j refers to the discrete optical depth measurements at wave numbers ν_j , measured values of optical depth are given as $\tau_m(\nu_j)$, $N_t = N + N_g$ is the sum of all droplet-size bins and absorbing gases, and N_v is the total number of discrete wave number measurements. Notice that no distinction between gas and droplet contributions to optical depth is made in Eq. (4) because $\sigma(S_k, \nu_j)$ simply refers to the extinction cross section at wave number ν_j for gas species or droplet-size bin S_k . One can arrive at (4) directly by minimizing the least-squares error between measured and modeled spectral optical depth or, equivalently, by treating Eq. (2) as a matrix equation, forming the so-called normal matrix equation by

multiplying both sides by the transpose of the theoretical cross-section matrix and performing Gauss–Seidel iteration³⁹ on this result. The physical interpretation of Eq. (4) is that the remainder after subtraction from the measured optical depth at all wave numbers of the contribution from all species except the k th is that portion of the optical depth that is due to the k th species.

Direct application of the iterative scheme in Eq. (4) often results in rough droplet-size spectra. Most inversion techniques have an explicit or implicit smoothing applied to them.¹⁶ The smoothing technique chosen was motivated by the simple algorithm described in Ref. 40. Smoothing is implemented by replacing $n_k^{(new)}$ in Eq. (4) with the weighted average of this value and its nearest neighbors,

$$n_k^{(new)} = \left(\frac{\alpha}{2}\right)n_{k-1}^{(old)} + (1 - \alpha)n_k^{(new)} + \left(\frac{\alpha}{2}\right)n_{k+1}^{(new)}, \quad (5)$$

where $0 \leq \alpha \leq 1$ is the weighting factor. Various amounts of smoothing can be implemented by adjusting the value of α . Three values of α have been investigated and are designated as smooth for $\alpha = 0.5$, semismooth for $\alpha = 0.25$, and not smoothed for $\alpha = 0$. The smoothing algorithm is not applied to gases, and end points of the droplet-size distributions were not smoothed. All retrieved spectra presented in Section 2 were computed using $\alpha = 0.5$ in Eq. (5).

Some details of our application of the iterative algorithm will perhaps be useful to others. FTIR measurements were performed at 289 wave numbers, although the narrow bands for CO₂ and plastic wrap absorption as shown in Fig. 1 were not included in the retrieval algorithm for measurements for which their effects on reducing the signal level to the noise level were obvious. A total of 129 droplet size bins were used, spanning a diameter range from 0.05 to 16 μm . The denominator and the first term in the numerator in Eq. (4) have to be computed only once before the iteration begins. Starting values for all droplet size bins and the water-vapor concentrations were all set to zero, although the routine seemed insensitive to the choice of starting values. Any new value after iteration was forced to zero if it was negative (positivity constraint). The measured water-vapor concentration shown in Fig. 2 was actually used in the retrieval algorithm. The algorithm was iterated 1000 times to reasonably ensure convergence, although as few as 30 iterations can provide adequate convergence for some applications. The theoretical droplet-extinction basis set given in Eq. (3) was computed using Simpson's rule for the integration, and Lorenz–Mie theory or anomalous diffraction theory was used for the theoretical extinction cross section²⁹ as discussed in Subsection 3.C.

B. Effects of Smoothing on the Retrieved Size Distributions

Figure 10 illustrates the effects of varying amounts of smoothing on the retrieved size spectrum. The

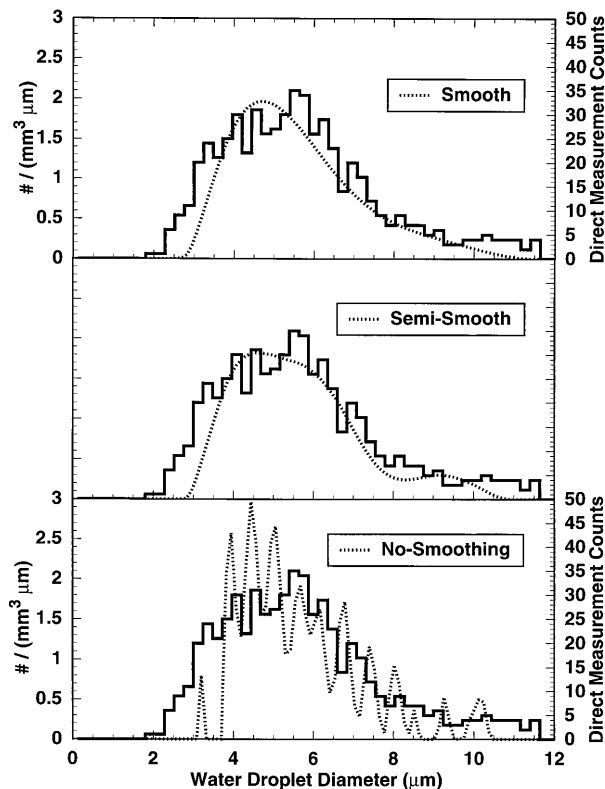


Fig. 10. Comparison of varying amounts of smoothing applied in the droplet-retrieval algorithm with the measured size spectrum to illustrate the nonuniqueness of size retrieval from a measured optical spectrum [lesser optical-depth curve in Fig. 4(a)]. Smoothing parameters of $\alpha = 0$ (no smoothing), $\alpha = 0.25$ (semi-smooth), and $\alpha = 0.5$ (smooth) were applied in the lower, middle, and upper panels, respectively. The directly measured size spectrum of Fig. 4(b) is shown to aid comparison.

smoothing parameter in Eq. (5) was $\alpha = 0$ for the lower panel (no smoothing), $\alpha = 0.25$ for the middle panel (some smoothing), and $\alpha = 0.5$ for the upper panel (more smoothing). These were all obtained from the lower optical-depth spectrum in Fig. 4(a). All three size spectra in Fig. 10 gave synthetic infrared spectra that overlie so closely that they are indistinguishable to the eye and are the same as the lower optical-depth synthetic spectrum in Fig. 4(a). In fact, the smoothed result in the upper panel of Fig. 10 is the dashed curve in Fig. 4(b).

The first three rows of Table 1 show quantities related to the first four moments of the retrieved distributions in Fig. 10 and the average error (square root of the summed squared error between modeled and measured IR spectra divided by the summed measured IR spectra) between measured and modeled optical-depth spectra. Good agreement exists among these quantities even though the various distributions shown in Fig. 10 are visually quite different.

Figure 10 and Table 1 clearly demonstrate the non-uniqueness aspect¹⁶ of droplet size retrieval from optical-depth measurements. More dramatic effects of smoothing have been observed in other retrieval

Table 1. Cloud Microphysical Properties and Error between Measured and Synthetic Optical-Depth

Theory	Concentration (mm ⁻³)	Mean Diameter (μm)	Mean Projection Area (μm ²)	Liquid Water (g/m ³)	Δρ _{vap} (g/m ³)	Average Error (%)
Lorenz-Mie α = 0	6.7	5.7	27.2	0.80	-0.79	2.0
Lorenz-Mie α = 0.25	6.8	5.6	26.8	0.80	-0.78	2.1
Lorenz-Mie α = 0.5	6.9	5.6	26.5	0.80	-0.78	2.2
Anomalous Diffraction α = 0.5	9.7	5.1	23.2	0.93	-1.88	3.7
Eq. (1)	-	-	-	0.72	-	-

schemes.⁴¹ The value α = 0.5 was used for the retrievals presented in Sec. 2 because it gave the most visually appealing spectra and yet was still able to diagnose bimodal spectra in other measurements.⁴²

C. Retrievals using Anomalous Diffraction Theory

Theoretical droplet-extinction cross sections for the retrieval were also computed by use of the simple anomalous diffraction theory for spheres²⁹ to examine how well an approximate theory performs in retrieving droplet-size and vapor concentrations. A number of retrieval schemes are based on analytical integration of the optical depth with anomalous diffraction theory for the theoretical extinction efficiency.^{7,23-28} The last row of Table 1 and Fig. 11 show the results of inverting optical-depth measurements with anomalous diffraction theory and of using the α = 0.5 smoothing factor. The synthetic optical-depth spectra is in relatively poor agreement with the measured spectrum in comparison with the Lorenz-Mie theory result shown as the lower optical depth in Fig. 4(a). The droplet-size spectrum is quite different from the Lorenz-Mie theory retrieval shown in the upper panel in Fig. 10. The total concentration, liquid-water content, and vapor concentration are in poor agreement with Lorenz-Mie theory results and liquid-water content as computed with Eq. (1), as shown in Table 1. The deviation of the liquid-water content retrieved from Lorenz-Mie theory is within 11% of value obtained from use of the single-wavenumber parameterization given in Eq. (1). This error is consistent with other laboratory measurements of liquid water content in fogs⁴³⁻⁴⁵ in which use of the parameterization was checked against mass measurement of collected cloud water, although use of anomalous diffraction theory is within 30% of the value computed from use of Eq. (1) and is inconsistent with other laboratory measurements.⁴³⁻⁴⁵

D. Significance of the Retrieved Size Distributions and Vapor Concentration: Evaporating Cloud Example

It is desirable to know the reliability of retrieved size distributions and vapor concentration. Suppose the spectral optical-depth contribution from one size bin or perhaps the vapor concentration is computed to form a reduced optical depth. The ratio of the summed reduced optical depth over all wave numbers to the summed total optical depth might be used as a measure of the significance of its contribution to the total optical depth. However, suppose that the contribution is from a hypothetical gas having only

one strong absorption band. The contribution to the total optical depth from such a hypothetical gas would be very important in the narrow absorption band, but would be completely negligible elsewhere. The spectral reduced and total optical depth should be multiplied by the spectral contribution in question before the sum is performed. The resulting quantity can be used to determine the significance of a particular contribution to the total optical depth given that the contribution might only add to the optical depth in discrete bands. The significance of contribution

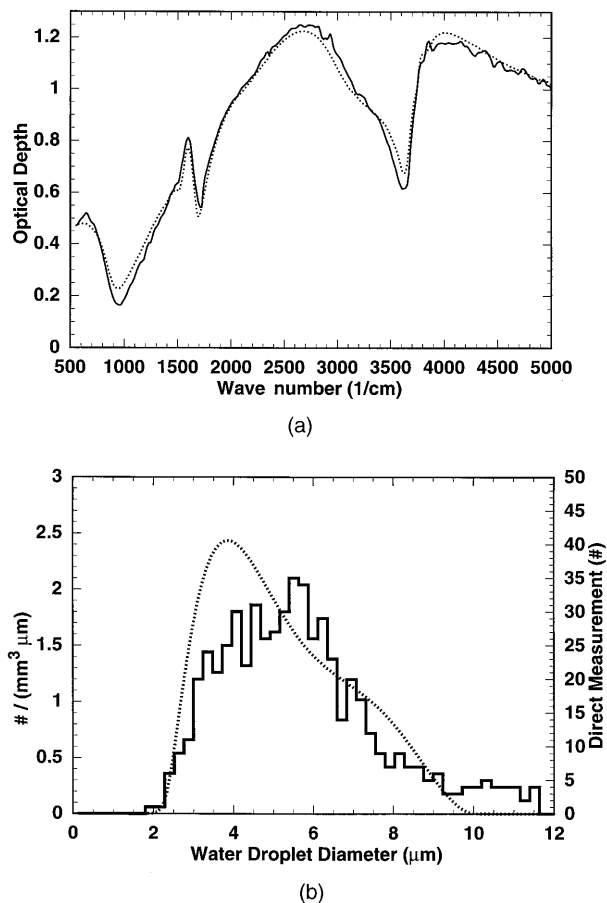


Fig. 11. (a) Optical depth as a function of wave number measured [solid curve, same as lesser optical-depth curve in Fig. 4(a)] and modeled (dotted curve) with anomalous diffraction theory. (b) Water droplet measured counts (solid curve) and concentration retrieved by inversion of the optical depth (dotted curve). The directly measured size spectrum of Fig. 4(b) is shown to aid comparison.

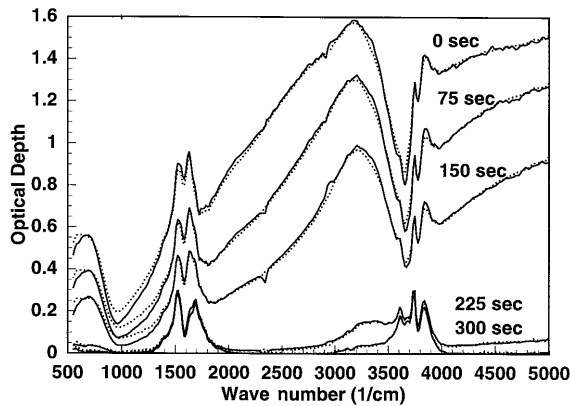


Fig. 12. Optical depth during fog evaporation [curves as in Fig. 4(a)].

S_k to the optical depth is denoted by $\text{Sig}(S_k)$, and is given by the equation

$$\text{Sig}(S_k) = n_k \frac{\sum_{j=1}^{N_v} \sigma(S_k, v_j)^2}{\sum_{j=1}^{N_v} \sigma(S_k, v_j) \tau_m(v_j)}. \quad (6)$$

In practice it has been useful to normalize significance to the maximum value.

The temporal evolution of an evaporating cloud was evaluated. A reference FTIR spectrum was taken when the chamber air was significantly undersaturated ($\text{RH} \approx 65\%$). (In contrast, chamber air was nearly saturated before the reference spectrum was taken for the dissipating cloud discussed in Sub-

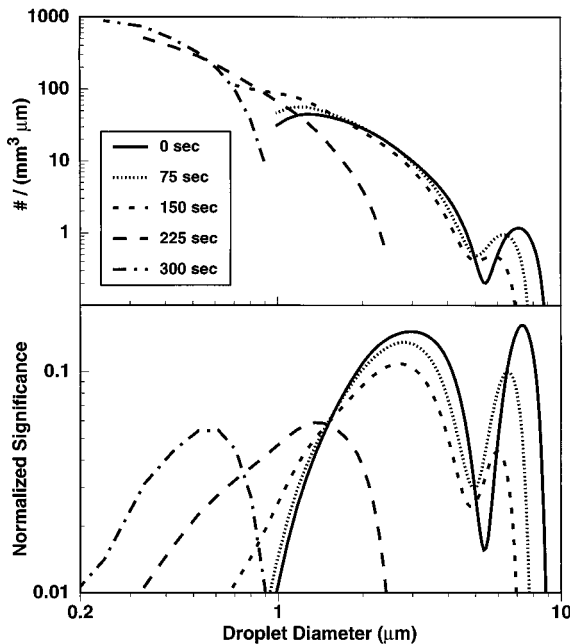


Fig. 13. Time-resolved droplet spectra retrieved from optical-depth measurements (upper panel) and normalized significance of droplet contribution to optical depth (lower panel) for an evaporating fog. Water-vapor normalized significance is unity.

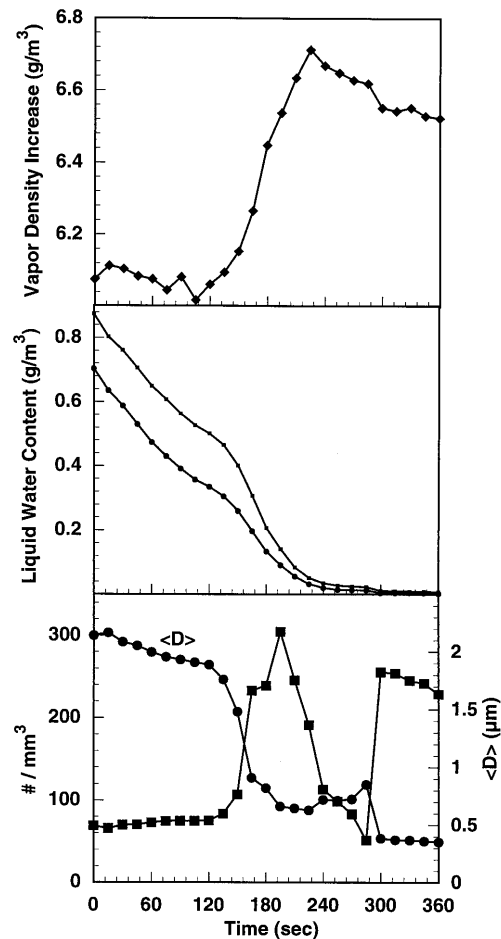


Fig. 14. Microphysical properties of the evaporating fog. The upper panel is vapor-density change, middle panel symbols are the same as in Fig. 8, and the lower panel symbols are the same as in Fig. 9. Curves are guides to the eye.

section 2.C.) Then the cloud from the ultrasonic nebulizer was added to the chamber until the optical depth, as monitored by a laser diode, was approximately unity. FTIR transmission spectra were performed at 15-s intervals as the cloud evaporated. Selected measured and retrieved optical-depth spectra during evaporation are shown in Fig. 12. The strong contribution of water vapor (refer to Fig. 2) to the total optical depth can be seen qualitatively in Fig. 12, particularly after 300 s of evaporation. A haze was still visually observable in the chamber after the last FTIR measurement was performed.

Retrieved droplet size spectra corresponding to the optical depth in Fig. 12 are shown in Fig. 13. A smoothing factor of $\alpha = 0.5$ was applied. The significance for water droplets as normalized to water vapor significance (which had the greatest significance in this case) is shown in the lower panel of Fig. 13. The contribution to the total optical depth from droplets with normalized significance < 0.01 was negligible, so all portions of the size spectra at or below this significance cutoff were forced to zero. The normalized significance can be used to determine the most reliable portions of a retrieved size spectrum. For

example, the size spectra obtained at 0 s is most reliable in the size ranges 2–4 μm and 7–8 μm . Note that, relative to water vapor, droplets are more significant at the beginning than at the end of the cloud evaporation, as one would expect.

Evidently many droplets with diameters less than 1 μm are in the chamber near the end of the measurement. Figure 14 shows that the peak concentration of $\approx 300 \text{ mm}^{-3}$ coincided with the peak vapor density caused by a sharp decrease in cloud liquid-water content. The mean droplet diameter was approximately 2.1 μm early on and dropped to $\sim 0.35 \mu\text{m}$ near the end as shown in the lower panel. The middle panel indicates relatively poor agreement on liquid-water content from use of the parameterization in Eq. (1) versus direct computation from the retrieved size distributions. This disagreement is likely due to a violation of the parameterization assumption. Key assumptions of the parameterization are that the droplet spectrum is sufficiently broad that a linear approximation of droplet extinction efficiency is appropriate and that droplet diameters are less than a maximum value.³⁷ The slope of the linear approximation for extinction efficiency underestimates the true slope for small-size parameters and overestimates it for large-size parameters.³⁷ Increasing the slope would have the effect of decreasing the coefficient 3.91 in Eq. (1), and hence would lower the liquid-water content estimate from the parameterization (squares in the middle panel of Fig. 14) toward the liquid-water content computed from the size spectra (circles in the same figure).

4. Conclusions

The ultimate utility of the technique presented for retrieving water-vapor concentration and droplet-size spectra of haze, fog, and cloud droplets will depend on the particle-size range and the accuracy of the assumed particle refractive index. For haze with only small (e.g., $< 0.1 \mu\text{m}$) particles, optical depth between 500 and 5000 cm^{-1} will begin to depend only on the liquid-water content and the absorption coefficient of water in the bulk and will be rather insensitive to the underlying size distribution. The same insensitivity begins to occur for droplet diameters larger than $\sim 50 \mu\text{m}$ because extinction begins to depend only on the total projected area, and spectrometer noise will eventually limit the ability to accurately measure the minuscule spectral variation. In addition, true extinction measurements for large droplets demand careful attention to the issue of the actual cone of radiation received by the detector. Errors in the assumed refractive index will produce errors in the retrieved vapor concentration.

The comparison of retrievals based on Lorenz–Mie theory and anomalous diffraction theory suggest that accurate retrieval of ice-crystal size distributions and water-vapor concentration from spectral extinction measurements³⁰ will depend strongly on the quality of the theoretical extinction cross section. This intercomparison also calls into question the validity of using anomalous diffraction theory to invert spectral

extinction measurements.^{7,23–27} Empirical parameterization of anomalous diffraction theory^{2,28} to bring it into closer agreement with the Lorenz–Mie theory should be performed.

Droplet retrieval from theoretical optical-depth spectra were considerably better than the retrievals based on measured optical-depth spectra. Measured optical depth was consistently lower near 1000 cm^{-1} and near 3700 cm^{-1} than the synthetic optical depth, as shown in Fig. 4(a) and as observed in all other inverted spectra not shown. Both of these spectral regions are near regions of maximum disagreement among the various compilations for the bulk refractive index of water shown in Fig. 3(a).

A key advantage of the spectral extinction inversion method for droplet size spectra estimation is that the cloud is minimally affected by the measurement in comparison with methods that require the cloud to be drawn into a device.

This work was supported by National Science Foundation grant ATM-9413437.

References

1. A. Arnulf, J. Bricard, E. Curé, and C. Vêret, "Transmission by haze and fog in the spectral region 0.35 to 10 microns," *J. Opt. Soc. Am.* **47**, 491–498 (1957).
2. D. Deirmendjian, "Atmospheric extinction of infrared radiation," *Q. J. R. Meteorol. Soc.* **86**, 371–381 (1960).
3. D. Deirmendjian, *Electromagnetic Scattering on Spherical Polydispersions* (Elsevier, New York, 1969), pp. 114–119.
4. V. E. Zuev, *Atmospheric Transparency in the Visible and Infrared* (Israel Program for Scientific Translations, Jerusalem, 1970), pp. 92–124.
5. E. J. McCartney, *Optics of the Atmosphere, Scattering by Molecules and Particles* (Wiley, New York, 1976), pp. 133–142.
6. V. E. Zuev, "Laser-light transmission through the atmosphere," in *Laser Monitoring of the Atmosphere*, E. D. Hinkley, ed. (Springer-Verlag, New York, 1976), pp. 55–56.
7. C. Tomasi and F. Tampieri, "Infrared radiation extinction sensitivity to the modified gamma distribution parameters for haze and fog droplet polydispersions," *Appl. Opt.* **15**, 2906–2912 (1976).
8. M. R. Clay, and A. P. Lenham, "Transmission of electromagnetic radiation in fogs in the 0.53–10.1- μm wavelength range," *Appl. Opt.* **20**, 3831–3832 (1981).
9. V. E. Zuev, *Laser Beams in the Atmosphere* (Plenum, New York, 1982), pp. 133–137.
10. V. Chimelis, "Extinction of CO_2 laser radiation by fog and rain," *Appl. Opt.* **21**, 3367–3372 (1982).
11. D. A. Stewart and O. M. Essenwanger, "A survey of fog and related optical propagation characteristics," *Rev. Geophys. Space Phys.* **20**, 481–495 (1982).
12. Z. S. Wu, K. F. Ren, and Y. P. Wang, "10.6 micron wave propagation in cloud, fog, and haze," *Int. J. Infrared Millim. Waves* **11**, 499–504 (1990).
13. M. E. H. van Dongen, H. J. Smolders, C. J. M. Braun, C. A. M. Snoeijs, and J. F. H. Willems, "Spectral light extinction to characterize fast fog formation," *Appl. Opt.* **33**, 1980–1988 (1994).
14. R. G. Eldridge, "Measurements of cloud drop-size distributions," *J. Meteorol.* **14**, 55–59 (1957).
15. R. G. Eldridge, "Haze and fog aerosol distributions," *J. Atmos. Sci.* **23**, 605–613 (1966).
16. S. Twomey, *Introduction to the Mathematics of Inversion in*

- Remote Sensing and Indirect Measurements* (Elsevier, New York, 1977), Chap. 5 and 6.
17. J. R. Bottiger, "Intercomparison of some inversion methods on systems of spherical particles," in *Advances in Remote Sensing Retrieval Methods*, A. Deepak, H. E. Fleming, and M. T. Chahine, eds. (Deepak, Hampton, Virginia, 1985), p. 587.
 18. R. Penndorf, "Comments on 'Measurements of cloud drop-size distributions,'" *J. Meteorol.* **14**, 573–574 (1957).
 19. R. G. Eldridge, "Measurements of cloud drop-size distributions: reply," *J. Meteorol.* **14**, 575–577 (1957).
 20. U. Amato, F. Esposito, C. Serio, G. Pavese, and F. Romano, "Inverting high spectral resolution aerosol optical depth to determine the size distribution of atmospheric aerosols," *Aerosol Sci. Technol.* **23**, 591–602 (1995).
 21. M. L. Clapp, R. E. Miller, and D. R. Worsnop, "Frequency-dependent optical constants of water ice obtained directly from aerosol extinction spectra," *J. Phys. Chem.* **99**, 6317–6326 (1995).
 22. P. R. Solomon, R. M. Carangelo, P. E. Best, J. R. Markham, and D. G. Hamblen, "Analysis of particle emittance, composition, size and temperature by FT-i.r. emission/transmission spectroscopy," *Fuel* **66**, 897–908 (1987).
 23. K. S. Shifrin and A. Ya. Perelman, "The determination of the spectrum of particles in a dispersed system from data on its transparency," *Opt. Spectrosc.* **15**, 285–289 (1963).
 24. A. Ya. Perelman and K. S. Shifrin, "Improvements to the spectral transparency method for determining particle-size distribution," *Appl. Opt.* **19**, 1787–1793 (1980).
 25. M. A. Box and B. H. J. McKellar, "Analytic inversion of multispectral extinction data in the anomalous diffraction approximation," *Opt. Lett.* **3**, 91–93 (1978).
 26. A. L. Fymat and C. B. Smith, "Analytical inversions in remote sensing of particle size distributions. 4: comparison of Fymat and Box-McKellar solutions in the anomalous diffraction approximation," *Appl. Opt.* **18**, 3595–3598 (1979).
 27. C. B. Smith, "Inversion of the anomalous diffraction approximation for variable complex index of refraction near unity," *Appl. Opt.* **21**, 3363–3366 (1982).
 28. J. D. Klett, "Anomalous diffraction model for inversion of multispectral extinction data including absorption effects," *Appl. Opt.* **23**, 4499–4508 (1984).
 29. H. C. van de Hulst, *Light Scattering by Small Particles* (Dover, New York, 1981), pp. 172–183.
 30. W. P. Arnott, Y. Y. Dong, and J. Hallett, "Extinction efficiency in the infrared (2–18 μm) of laboratory ice clouds: observations of scattering minima in the Christiansen bands of ice," *Appl. Opt.* **34**, 541–551 (1995).
 31. R. G. Fleagle and J. A. Businger, *An Introduction to Atmospheric Physics* (Academic, New York, 1963), pp. 81–91.
 32. H. D. Downing and D. Williams, "Optical constants of water in the infrared," *J. Geophys. Res.* **80**, 1656–1661 (1975).
 33. G. M. Hale and M. R. Querry, "Optical constants of water in the 200-nm to 200- μm wavelength region," *Appl. Opt.* **12**, 555–563 (1973).
 34. V. M. Zolotarev, B. A. Mikhailov, L. I. Aperovich, and S. I. Popov, "Dispersion and absorption of water in the infrared," *Opt. Spectrosc.* **27**, 430–432 (1969).
 35. D. M. Wieliczka, S. Weng, and M. R. Querry, "Wedge-shaped cell for highly absorbent liquids: infrared optical constants of water," *Appl. Opt.* **28**, 1714–1719 (1989).
 36. B. J. Mason, *The Physics of Clouds* (Clarendon, Oxford, 1971), pp. 93–94.
 37. P. Chylek, "Extinction and liquid water content of fogs and clouds," *J. Atmos. Sci.* **35**, 296–300 (1978).
 38. R. G. Pinnick, S. G. Jennings, P. Chylek, and H. J. Auvermann, "Verification of a linear relation between IR extinction, absorption, and liquid water content of fogs," *J. Atmos. Sci.* **36**, 1577–1586 (1979).
 39. R. L. Burden and J. D. Faires, *Numerical Analysis* (PWS, Boston, 1993) 410–411.
 40. G. R. Markowski, "Improving Twomey's algorithm for inversion of aerosol measurement data," *Aerosol Sci. Technol.* **7**, 127–141 (1987).
 41. P. T. Walters, "Practical applications of inverting spectral turbidity data to provide aerosol size distributions," *Appl. Opt.* **19**, 2353–2365 (1980).
 42. W. P. Arnott, C. Schmitt, Y. Liu, and J. Hallett, "Laboratory FTIR measurements of ice crystal and water droplet clouds: particle size spectrum inversion," in *Proceedings of the Twelfth International Conference on Clouds and Precipitation* (Page Bros., Norwich, 1996), pp. 990–992.
 43. A. W. Gertler and R. L. Steele, "Experimental verification of the linear relationship between IR extinction and liquid water content of clouds," *J. Appl. Meteorol.* **19**, 1314–1317 (1980).
 44. D. Bruce, C. W. Bruce, Y. P. Yee, L. Cahenzli, and H. Burket, "Experimentally determined relationship between extinction coefficients and liquid water content," *Appl. Opt.* **19**, 3355–3360 (1980).
 45. P. F. Nolan and S. G. Jennings, "Extinction and liquid water content measurements at CO₂ laser wavelengths," *J. Atmos. Oceanic Technol.* **4**, 391–400 (1987).